

Ordered Mesoporous TiO₂/Activated Carbon for Adsorption and Photocatalysis of Acid Red 18 Solution

Ji Zhang,^a Fu Liu,^a Jianmin Gao,^{a,*} Yao Chen,^{a,*} and Xinmin Hao^b

Ordered mesoporous TiO₂, loaded on walnut shell-based activated carbon, was prepared *via* sol-gel and ultrasonic-assisted technology. The obtained composites (M-TiO₂/AC) were characterized *via* X-ray diffraction, N₂ adsorption-desorption isotherms, and Fourier transform infrared spectroscopy. The adsorption-photocatalytic reduction capabilities were calculated using the removal rate of Acid Red 18 solution *via* UV spectrophotometry. The specific area of M-TiO₂/AC increased from 563 m²·g⁻¹ to 881 m²·g⁻¹, compared to TiO₂/AC. The removal rate was 92.3% when the Acid Red 18 with a concentration of 80 mg·L⁻¹ was subjected to illumination for 2 h with 0.15 g of M-TiO₂/AC. Under this condition the removal rate of Acid Red 18 solution by M-TiO₂/AC was higher than that of TiO₂/AC (83.7%), or AC (73.1%), which was attributed to the regular mesoporous structure, pore-pore synergistic amplification, and TiO₂ photocatalysis. Acid Red 18 might be oxidized and decomposed into small molecular substances, such as CO₂ and H₂O, by strong oxidizing free hydroxyl radicals provided during the photocatalytic process by M-TiO₂. The adsorption and photocatalytic processes followed the pseudo-second-order kinetic model. Internal diffusion and external diffusion processes influenced the adsorption rate.

Keywords: Ordered mesoporous TiO₂; Activated carbon; Acid Red 18; Adsorption; Photocatalysis

Contact information: a: Ministry of Education (MOE) Key Laboratory of Wooden Material Science and Application, Beijing Key Laboratory of Lignocellulosic Chemistry, MOE Engineering Research Centre of Forestry Biomass Materials and Bioenergy, Beijing Forestry University, 35 Qinghua East Road, Haidian, Beijing 100083 China; b: The Research Center of China-hemp Materials, The Quartermaster Research Institute of the General Logistics Department of the PLA, 28 Xizhimen North Street, Beijing 100088 China; *Corresponding author: jmgao@bjfu.edu.cn

INTRODUCTION

Dyes are widely used in a variety of industries, such as textile, printing, and paper. The resulting dye wastewater, which contains a variety of poisonous and harmful substances, is a main environmental and industrial pollutant (Li *et al.* 2014). Azo dyes, the largest class of dyes, are widely applied to the textile and printing industries (Senthilraja *et al.* 2015). Acid Red 18 is a commonly used azo acid dye, which contains an -N=N- group that is conjugated with aromatic systems. Its effective degradation is difficult in the environment, rendering it a severe source of pollution (Xu *et al.* 2013).

The photocatalysis technique has been reported to have many applications in wastewater treatment, such as antibacterial effects, self-cleaning ability, *etc.* It can provide a potentially inexpensive and convenient method to treat organic and inorganic contaminants and eventually degrade these compounds to water, carbon dioxide, and harmless inorganic matters (Omri *et al.* 2014). Among all of the nano-photocatalytic materials, titanium dioxide (TiO₂) becomes the most promising photocatalyst due to its strong oxidation activity, stability, and nontoxicity (Qian *et al.* 2016). In the present study,

ordered mesoporous oxides have been demonstrated to be the more effective photocatalysts and widely applied in various fields (Mittal *et al.* 2009; Saravanan *et al.* 2014). Mesoporous TiO₂, which has developed an ordered channel structure, not only can make up for the reduction of carrier surface area, but also can enhance the photocatalytic efficiency *via* pore-pore synergistic amplification effects between carrier and mesoporous TiO₂, when compared to nonporous TiO₂ (Li *et al.* 2013).

However, TiO₂ has two main disadvantages: low quantum yield and low photocatalytic activity. The coupling of TiO₂ with carbon-based materials is favorable to overcome these disadvantages (Gupta *et al.* 2012). Compared to some expensive carbon materials such as nanotubes and graphene, activated carbon (AC) is extensively used for waste gas disposal, and for water and industrial residue due to its well-developed pore structure and excellent related adsorption properties (Mittal *et al.* 2012; Zhang *et al.* 2013). Activated carbon can be produced from a variety of raw materials, and forestry and agricultural residues are a particularly good choice from both economical and environmental standpoints in addition to their abundant availability (Zhang *et al.* 2015). Titanium dioxide can be loaded onto active carbon, which can improve its photocatalytic efficiency, thus lowering the treatment cost. However, loading with TiO₂ can result in the substantial blocking of carrier pores and a consequent decrease of carrier surface area and absorption efficiency (Singh *et al.* 2016). Using ordered mesoporous TiO₂ which has large surface area and ordered pore networks instead of nonporous TiO₂ coupled with activated carbon is favorable to overcome these disadvantages. This approach can increase surface reactive sites and improve mass transport in photocatalysis (Ahmaruzzaman *et al.* 2011; Saleh *et al.* 2012).

In this study, ordered mesoporous TiO₂/AC composite photocatalytic materials were prepared, utilizing cetyltrimethylammonium bromide (CTAB) as a surfactant template and tetrabutyl titanate as a pore-making reagent and titanium source. The obtained composite materials were characterized *via* X-ray diffraction (XRD), N₂ adsorption-desorption isotherms, and Fourier transform infrared (FTIR) spectroscopy. Furthermore, their adsorption and photocatalytic capabilities as well as the conditions of Acid Red 18 were analyzed *via* UV spectrophotometry.

EXPERIMENTAL

Materials

Walnut shells were harvested from the Hebei province in Handan, China. The tetrabutyl titanate and CTAB were purchased from the Beijing Chemical Works (Beijing, China). Anhydrous ethanol (Shanghai Chemical Reagent Company, Shanghai, China) was of analytical grade.

Preparation of ordered mesoporous TiO₂/activated carbon

For the carbonization step, the walnut shells were heated at a temperature increase rate of 10 °C/min to a final temperature of 500 °C in a nitrogen atmosphere, which was retained for 1 h. Subsequent to carbonization, the sample was crushed. The particle sample was soaked in potassium hydroxide (KOH) solution of 50% concentration for 24 h, then oven-dried at 103 °C ± 2 °C *via* an electricity heat drum wind drying oven (Taisitee, 101-1AB, Tianjin, China) until a constant weight was reached. The mass ratio of KOH/samples was 3:1. In the activation step, the KOH-impregnated sample was

heated at a rate of 20 °C/min to a final temperature of 800 °C that was retained for 1 h in a nitrogen atmosphere. Finally, this sample was repeatedly washed with hot distilled water until the pH of the solution reached approximately 6 to 7, then was oven-dried at 103 °C ± 2 °C until a constant weight was reached. The obtained powdery material was activated carbon (AC).

The ultrasonic-sol-gel method was used to prepare TiO₂/AC. Then, 0.5 g AC was dispersed into a mixture of 10 mL tetrabutyl titanate and 40 mL anhydrous ethanol under continuous stirring until a homogeneous sol (A) was formed. Next, 2 mL of distilled water were added to 10 mL of anhydrous ethanol, and the pH of the solution was adjusted from 2 to 3 with concentrated hydrochloric acid. The obtained solution was subjected to magnetic stirring for 30 min until it formed a homogeneous sol (B). Sol (B) was added to sol (A) and the mixture was subsequently maintained in the ultrasonic device for 2 h. The obtained sol was further aged for 24 h, then was oven-dried at 103 °C ± 2 °C for 6 h. The obtained mixture was heated at a rate of 20 °C/min to a final temperature of 500 °C, which was retained for 2 h. The resulting composite was filtered and repeatedly washed with anhydrous ethanol and distilled water, then oven-dried at 103 °C ± 2 °C for 6 h. The obtained powdery material was TiO₂/activated carbon (TiO₂/AC). TiO₂ content of TiO₂/AC could reach 44.6% through the calculation of calcination method.

Next, 0.5 g AC was dispersed into a mixture of 10 mL Ti(C₄H₉O)₄ and 40 mL anhydrous ethanol to form a homogeneous sol (A) under continuous stirring. An amount of 1.8 g of CTAB was fully dissolved in 10 mL of anhydrous ethanol. Then, 2 mL of distilled water were added and the pH was adjusted from 2 to 3 with concentrated hydrochloric acid. The obtained solution was subjected to magnetic stirring for 30 min to form the soft template (ST). The ST was added to sol (A), and then maintained in the ultrasonic device for 2 h. The obtained sol was further aged for 24 h and was oven-dried at 103 °C ± 2 °C for 6 h. The obtained mixture was heated at a rate of 20 °C/min to a final temperature of 500 °C that was retained for 2 h. The resulting composite was filtered and repeatedly washed with anhydrous ethanol and distilled water, then oven-dried at 103 °C ± 2 °C for 6 h. The obtained powdery material was ordered mesoporous TiO₂/activated carbon (M-TiO₂/AC). TiO₂ content of M-TiO₂/AC could reach 43.9% through the calculation of calcination method.

Methods

Characterization of M-TiO₂/AC

Wide-angle X-ray diffraction curves and small Shimadzu -angle X-ray diffraction curves were investigated *via* an X-ray diffractometer (Shimadzu, XRD-6000, Shimadzu, Kyoto, Japan) with a Cu K α radiation source ($\lambda = 0.15418$ nm) at 40 kV.

Nitrogen sorption isotherms were determined at 77 K with a Micromeritics ASAP 2020 sorption analyzer (Quantachrome, Autosorb-iQ2-MP, Houston, America). The Brunner–Emmet–Teller (BET) calculation method was utilized to calculate the specific surface areas according to the adsorption branch of the isotherms. The total pore volume was defined as the volume of liquid nitrogen, corresponding to the amount adsorbed at a relative pressure of $p/p_0 = 0.99$.

The chemical characterization of the functional groups of the samples was investigated *via* a Fourier transform infrared spectrometer (Bruker, Tensor27, Karlsruhe, Germany) in the 4000 cm⁻¹ to 400 cm⁻¹ range and adopting pellets with samples dispersed in potassium bromide (KBr).

Photocatalytic reduction of Acid Red 18

In photocatalytic degradation experiments of Acid Red 18, different amounts of the sample (0.05 g, 0.10 g, 0.15 g, 0.20 g, 0.25 g, and 0.30 g) were added to 250 mL of the Acid Red 18 solution to achieve a certain concentration (20 mg/L, 40 mg/L, 60 mg/L, 80 mg/L, 100 mg/L, and 120 mg/L, respectively). After the reaction at 25 °C in ultraviolet irradiation for 2 h with an ultraviolet lamp (Jingke, WHF-204B, Shanghai, China), the sample particles were filtered *via* 0.45 μm membranes. Then, the absorbance of the filtrate was tested *via* UV-spectrophotometer at a wavelength of 503 nm. The residual concentration of Acid Red 18 solution could be calculated *via* the standard curve of absorbance and concentration of Acid Red 18 solution. The experiment was repeated thrice and the averages of all results were calculated.

RESULTS AND DISCUSSION

X-ray Diffraction

Figure 1 shows the wide-angle X-ray diffraction curves of the samples. This result clearly revealed the presence of nanocrystalline anatase from TiO_2 and TiO_2/AC , based on seven high-intensity crystal peaks at $2\theta = 25^\circ$ to 75° (25.1° , 38.0° , 47.5° , 53.5° , 55.1° , 62.5° , and 75°) that were observed and indexed as (101), (004), (200), (105), (211), (204), and (215), respectively. These peaks are clear characteristics of anatase TiO_2 . Similar crystal peaks of nanocrystalline anatase were observed in the X-ray diffraction curves of M- TiO_2 and M- TiO_2/AC . Furthermore, they still had crystal faces (110), (101), (111), (220), and (310) that corresponded to the five diffraction peaks of rutile with $2\theta = 25^\circ$ to 65° (27.5° , 36.5° , 41.0° , 56.5° , and 64.5°) rutile. These results clearly revealed the presence of anatase and rutile crystalline phases from M- TiO_2 and M- TiO_2/AC . This was mainly due to the addition of CTAB, which promoted the conversion of TiO_2 nanoparticles from anatase to rutile. It is well known that the main active crystal phases of TiO_2 are anatase and rutile. Furthermore, according to Ambrus *et al.* (2008), photocatalysts containing anatase and rutile phases are more efficient than those with the anatase phase only.

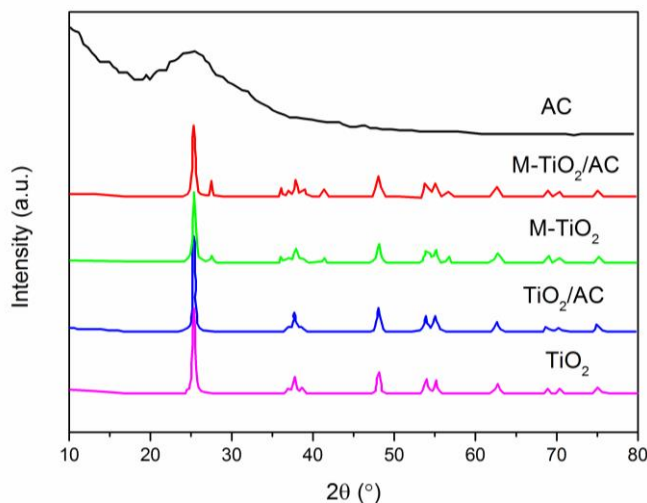


Fig. 1. Wide-angle X-ray diffraction curves of samples

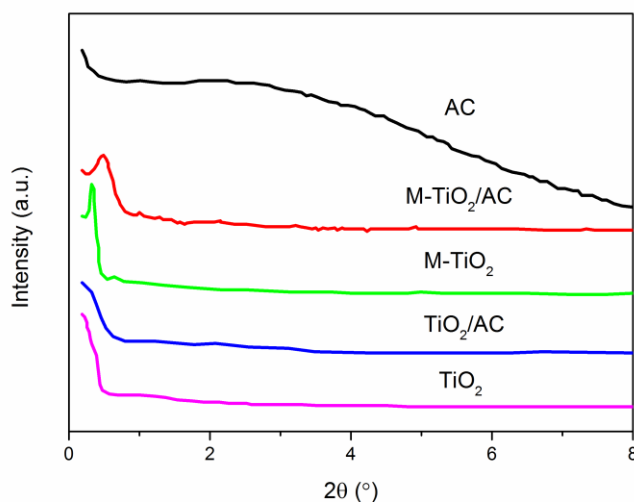


Fig. 2. Small-angle X-ray diffraction curves of samples

The typical small-angle X-ray diffraction curves of the mesoporous samples are apparent in Fig. 2. A half-peak was found at approximately 0.2° to 0.6° from the curve of TiO_2 and TiO_2/AC , which revealed that TiO_2 and TiO_2/AC possessed a little organized mesoporous structure. One clear peak at approximately 0.5° was observed in the pattern of M-TiO_2 . This result revealed that M-TiO_2 had a high ordered mesoporous structure that was mainly due to the pore-forming role of ST. Compared to M-TiO_2 , the diffraction peak of $\text{M-TiO}_2/\text{AC}$ shifted to the right and its intensity weakened, which was mainly due to the shrinkage of the pores and reduction of the order degree of the mesoporous TiO_2 in the calcination process after the mixture of M-TiO_2 and AC (Chandraboss *et al.* 2016).

Porous Texture

Figures 3 and 4 show N_2 adsorption–desorption isotherms and the corresponding Barrett-Joyner-Halenda (BJH) pore-size distribution plots of the samples. The N_2 adsorption-desorption isotherm of AC exhibited type I characteristics that indicated its microporous features, which coincided with a relatively sharp peak at pore diameters below 2 nm. The curves of M-TiO_2 and $\text{M-TiO}_2/\text{AC}$ exhibited small hysteresis loops, revealing type IV isotherms, which are representative of mesoporous materials (Yu *et al.* 2007). In addition, they also had a narrow BJH adsorption pore size distribution with a mean value of 13 nm, which implied that the materials had very regular pore channels in the mesoporous region and confirmed that M-TiO_2 had a clear absorption hysteresis loop and typical mesoporous distribution (8 nm to 18 nm). Furthermore, after M-TiO_2 went through the AC load, the hysteresis loop of the N_2 adsorption-desorption curve still existed and the noticeable increase of the adsorption volume of N_2 revealed that $\text{M-TiO}_2/\text{AC}$ had a large amount of mesopores and a higher specific surface area. The N_2 adsorption-desorption isotherm of TiO_2 exhibited type II characteristics and the adsorption capacity had not considerably changed for P/P_0 below 0.2. This confirmed that TiO_2 had hardly any micropores and mesopores (Fu *et al.* 2015). Furthermore, there was no peak in the pore size distribution pattern of TiO_2 suggesting that TiO_2 was a pore-free material.

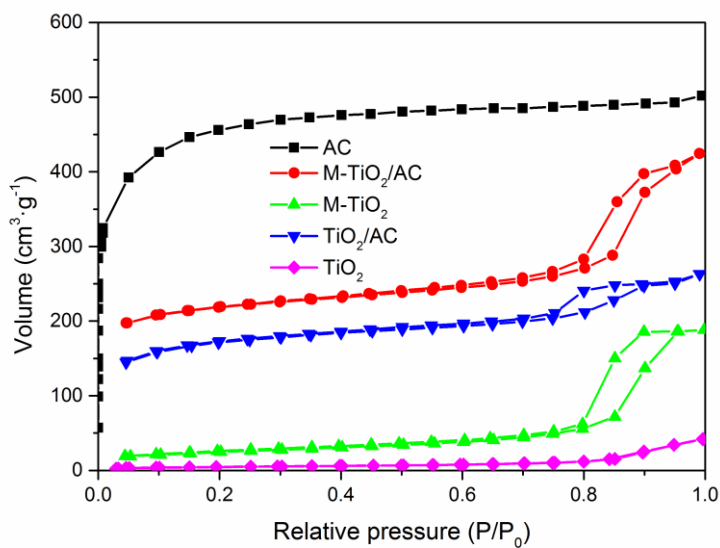


Fig. 3. N₂ adsorption-desorption isotherms of samples

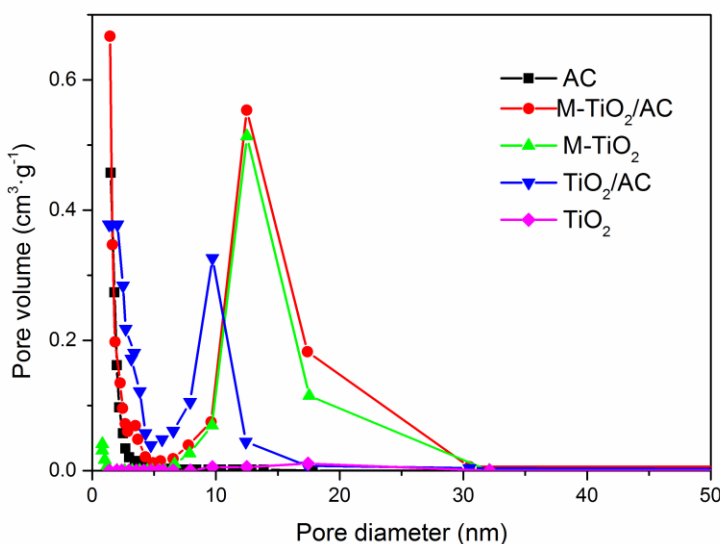


Fig. 4. Pore size distribution of samples

As shown in Table 1, AC had the largest specific area of $1552 \text{ m}^2 \cdot \text{g}^{-1}$. When AC was loaded with TiO_2 , the specific area of the TiO_2/AC was reduced to $563 \text{ m}^2 \cdot \text{g}^{-1}$, which was mainly due to the load with TiO_2 causing a substantial blockage of carrier pores. However, when the AC was loaded with M-TiO_2 , the specific area of the $\text{M-TiO}_2/\text{AC}$ reached $881 \text{ m}^2 \cdot \text{g}^{-1}$, which was mainly due to an ordered mesoporous structure and a large specific area ($112 \text{ m}^2 \cdot \text{g}^{-1}$) of M-TiO_2 in the pore-pore load. This was favorable for the growth of adsorption and photocatalytic capability for organic pollutants. In addition, compared to TiO_2 , the average crystallite sizes of TiO_2/AC and $\text{M-TiO}_2/\text{AC}$ decreased, which was mainly attributed to the noncrystalline layer of AC impeding the growth of TiO_2 crystal particles and the collapse of pore walls (Liu *et al.* 2015).

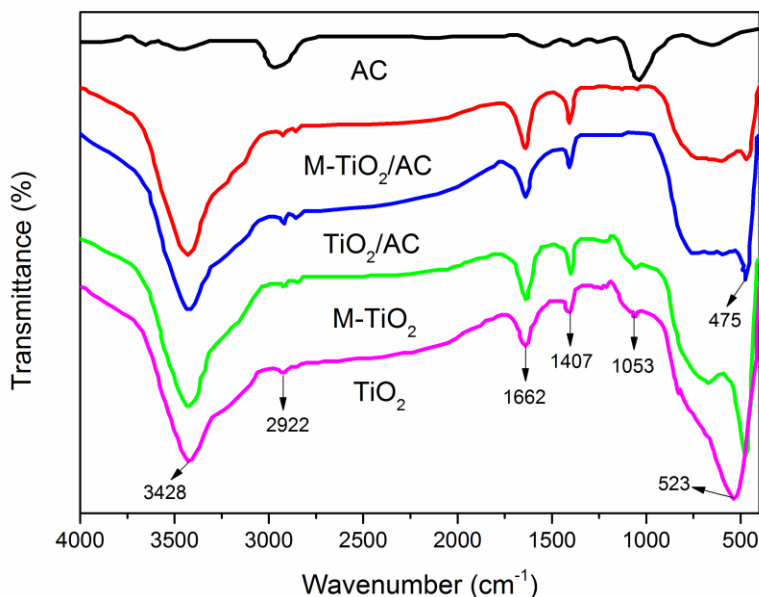
Table 1. Pore Structure Characteristics of Samples

Samples	Average Crystallite Size (nm)	S_{BET} ($\text{m}^2\cdot\text{g}^{-1}$)	V_{total} ($\text{cm}^3\cdot\text{g}^{-1}$)	Dp (nm)
AC	-	1552	0.78	2.01
M-TiO ₂ /AC	17.7	881	0.62	3.01
M-TiO ₂	17.8	112	0.28	12.45
TiO ₂ /AC	18.1	563	0.42	2.80
TiO ₂	20.5	13	-	-

Note: The average crystallite size is calculated via the Scherrer Equation; S_{BET} : BET specific surface area; V_{Total} : total pore volume; and Dp: average pore diameter

FTIR Spectral Analysis

The FTIR characterization of samples is shown in Fig. 5. The spectra of all of the samples (except AC) indicated a surface hydroxyl group (Ti-OH) that absorbed infrared radiation at 3428 cm^{-1} and 1662 cm^{-1} (Kuo *et al.* 2011). The stretching vibration of Ti-O-Ti was found at approximately 523 cm^{-1} and 475 cm^{-1} (Liu *et al.* 2007), which was caused by the presence of TiO₂ and M-TiO₂. Furthermore, the peaks observed at 2922 cm^{-1} , 1407 cm^{-1} , and 1053 cm^{-1} suggested that the vibration of Ti-O-C came from the direct hydration of $\text{Ti}(\text{C}_4\text{H}_9\text{O})_4$ and attachment on AC, which was favorable to improve the photocatalytic activity of the samples (Fu *et al.* 2016). In addition, compared to TiO₂ and M-TiO₂, TiO₂/AC and M-TiO₂/AC composites did not show a new absorption peak. This suggested that there was minimal new chemical bonding between TiO₂/M-TiO₂ and activated carbon in the process of synthesis.

**Fig. 5.** FTIR spectra of samples

Effect of Contact Time

TiO₂-AC was prepared by a physical mixture of AC and TiO₂, in which the mass ratio of AC and TiO₂ was 1:1. (Matos, J. *et al.* 1998). As shown in Fig. 6, the removal rate of the Acid Red 18 from different samples had initially and quickly increased and then favored gradually towards stabilization with increased time. The Acid Red 18 removal rates of M-TiO₂/AC and TiO₂/AC reached 92.3% and 83.7%, respectively, within 120 min. These values were all higher than those of AC, M-TiO₂, and TiO₂, especially compared to AC.

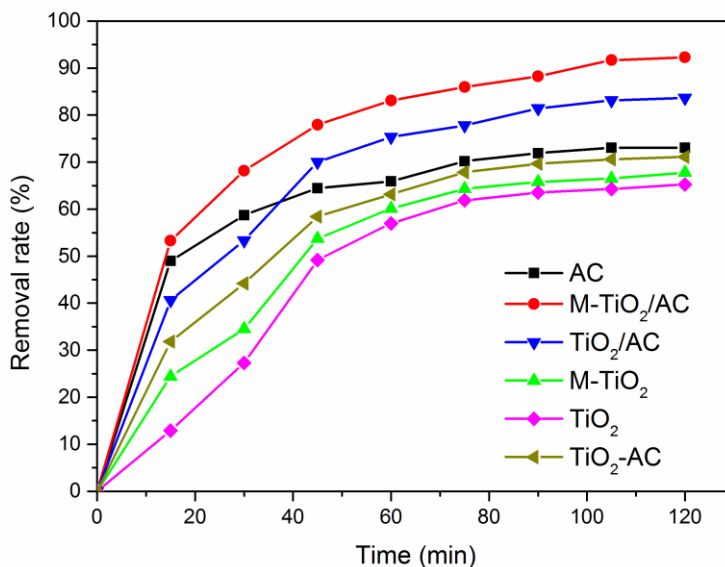


Fig. 6. Effect of contact time on adsorption of Acid Red 18 solution with illumination (Acid Red 18 concentration = 80 mg·L⁻¹; sample dosage = 0.15 g)

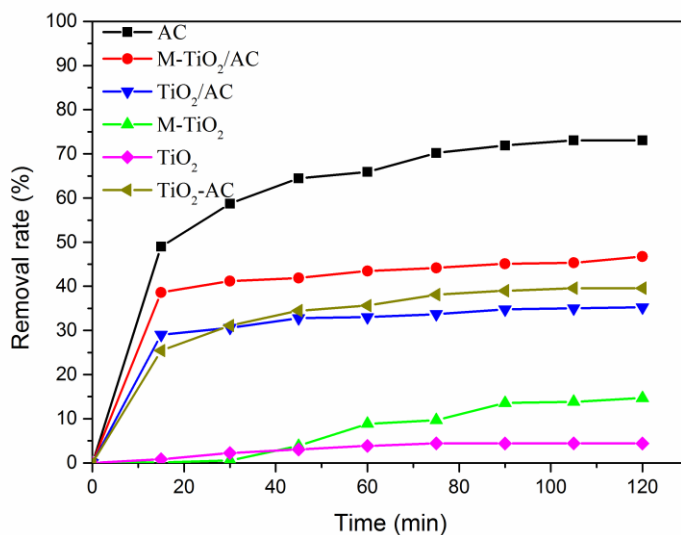


Fig. 7. Effect of contact time on adsorption of Acid Red 18 solution without illumination (Acid Red 18 concentration = 80 mg·L⁻¹; sample dosage = 0.15 g)

Although the specific surface area of M-TiO₂/AC decreased, the M-TiO₂ decomposed Acid Red 18 much more efficiently with illumination. Moreover, the pore-pore synergistic amplification effect, which occurred between AC and ordered mesoporous TiO₂, promoted Acid Red 18 particles to concentrate at the TiO₂ surface, which was conducive to accelerate the rate of photocatalytic degradation (Wu *et al.* 2016).

As shown in Fig. 7, the Acid Red 18 removal rate of AC was noticeably higher than that in other adsorbents without illumination, which was mainly due to the huge specific surface area and developed microporous structure of AC that was advantageous to the adsorption of Acid Red 18. Moreover, the M-TiO₂/AC and TiO₂/AC composites had almost no photocatalytic abilities without illumination. Compared with AC, these composites had less porosity and specific surface area as loading TiO₂ on AC.

Adsorption Kinetic Studies

As shown in Fig. 8 and Table 2, all experimental kinetic data were calculated *via* the pseudo-first-order kinetics (Eq. 1), pseudo-second-order kinetics (Eq. 2), and the intraparticle pore diffusion model 3.

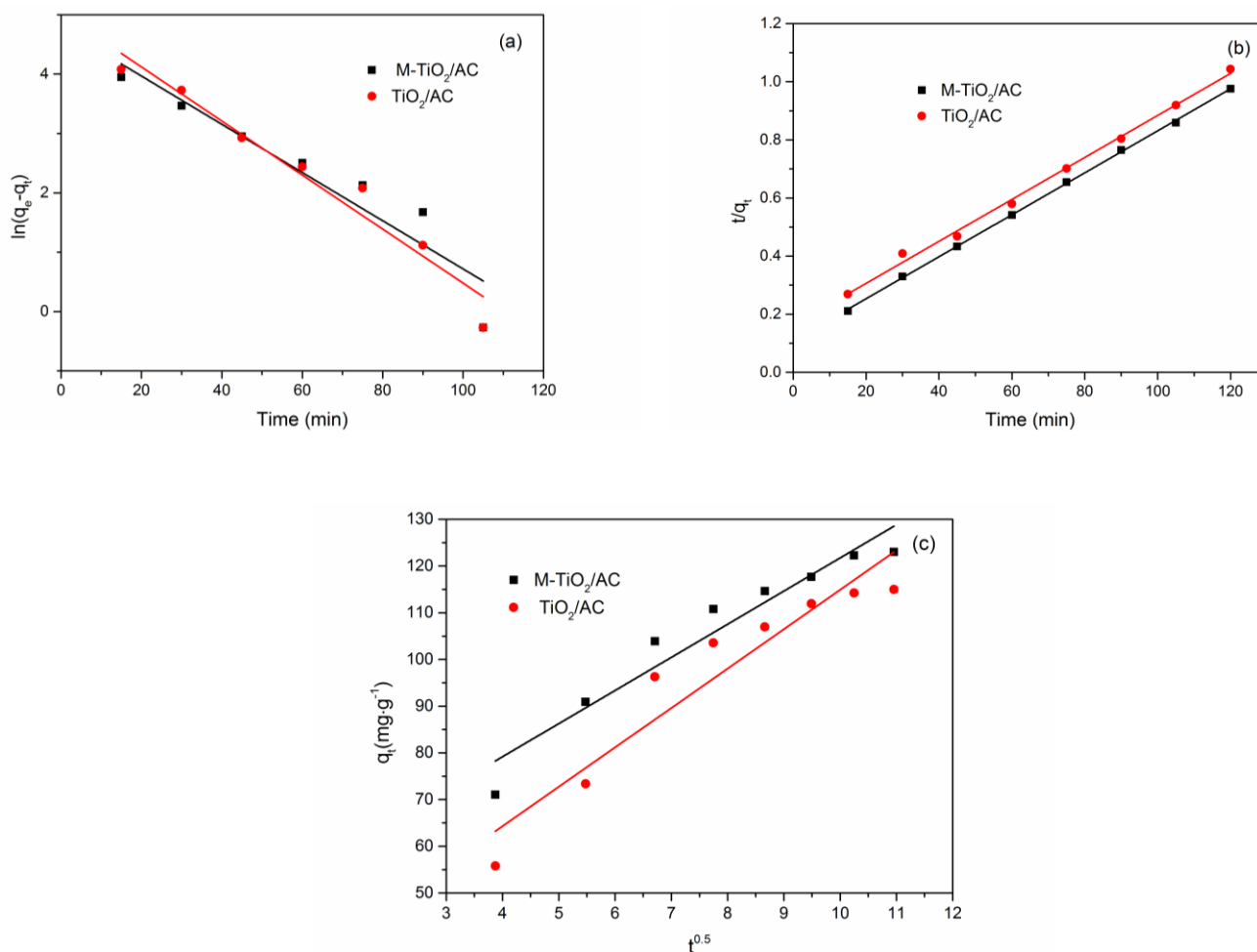


Fig. 8. Pseudo-first-order (a), pseudo-second-order (b), and intraparticle pore diffusion model (c) sorption kinetics curves

Table 2. Pseudo-first-order Kinetics, Pseudo-second-order Kinetics, and Intraparticle Pore Diffusion Model Parameters

Samples	Pseudo-first-order Kinetics			Pseudo-second-order Kinetics			Intraparticle Pore Diffusion Model		
	q_e ($\text{mg}\cdot\text{g}^{-1}$)	k_1 (min^{-1})	R^2	q_e ($\text{mg}\cdot\text{g}^{-1}$)	k_2	R^2	k_{ip}	C	R^2
M-TiO ₂ /AC	119.2	0.041	0.90	138.9	0.0005	0.996	10.8	19.3	0.91
TiO ₂ /AC	153.3	0.046	0.96	138.9	0.0003	0.999	10.7	11.6	0.94

Note: q_e : the amount of Acid Red 18 adsorbed at equilibrium area; k_1 : the pseudo-first-order kinetics rate constant; k_2 : the pseudo-second-order kinetics rate constant; k_{ip} : the intraparticle pore diffusion rate constant; C : the intercept that represented the thickness of boundary layer effect; and R^2 : regression coefficient

These kinetics equations were written as follows,

$$\ln(q_e - q_t) = \ln q_e - k_1 t \quad (1)$$

$$t / q_t = 1 / (k_2 \times q_e^2) + t / q_e \quad (2)$$

$$q_t = k_{ip} t^{1/2} + C \quad (3)$$

where q_t is the amount of Acid Red 18 ($\text{mg}\cdot\text{g}^{-1}$) adsorbed at time t (min), q_e is the amount of Acid Red 18 ($\text{mg}\cdot\text{g}^{-1}$) adsorbed at equilibrium, k_1 and k_2 are rate constants of pseudo-first-order (min^{-1}) and pseudo-second-order kinetics model ($\text{g}\cdot\text{mg}^{-1}\cdot\text{min}^{-1}$), respectively, and k_{ip} is the intraparticle pore diffusion rate constant ($\text{mg}\cdot\text{g}^{-1}\cdot\text{min}^{-1}$).

It can clearly be seen that the coefficients of determination (R^2) of M-TiO₂/AC and TiO₂/AC in the pseudo-second-order kinetics equation were both higher than those in the pseudo-first-order kinetics equation. These characteristics indicated that the removal process of Acid Red 18 solution was more suited to be described by the pseudo-second-order model (Zhang *et al.* 2011). Furthermore, the linear relationships of M-TiO₂/AC and TiO₂/AC with the intraparticle pore diffusion model were both less obvious indicating that intraparticle diffusion influenced the adsorption mass transfer process, although this was not the only factor. Internal and external diffusion worked simultaneously in the adsorption process (Xue *et al.* 2011; Hubbe *et al.* 2012).

Effect of Acid Red 18 Initial Concentration

As depicted in Fig. 9, the removal rate of Acid Red 18 decreased from 20 $\text{mg}\cdot\text{L}^{-1}$ to 120 $\text{mg}\cdot\text{L}^{-1}$ with increased initial concentration. This was attributed to the saturated adsorptive capacity of AC as well as to the excessively high initial concentration of Acid Red 18 solution obstructing the transmittance of ultraviolet light, consequently reducing the photocatalytic efficiency of M-TiO₂ and TiO₂. Synthetical consideration of the removal rate of Acid Red 18 revealed 80 $\text{mg}\cdot\text{L}^{-1}$ as the most suitable initial concentration of Acid Red 18 solution.

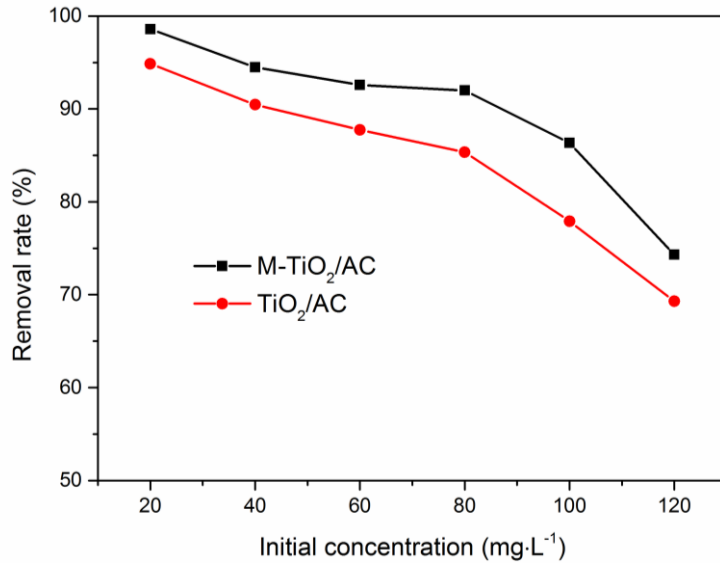
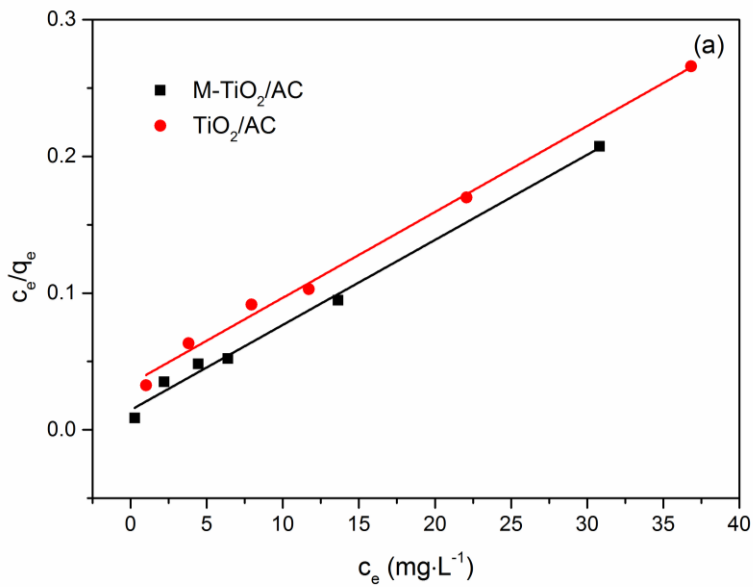


Fig. 9. Effect of initial concentration for adsorption of Acid Red 18 solution (sample dosage = 0.15 g)

Adsorption Isotherms



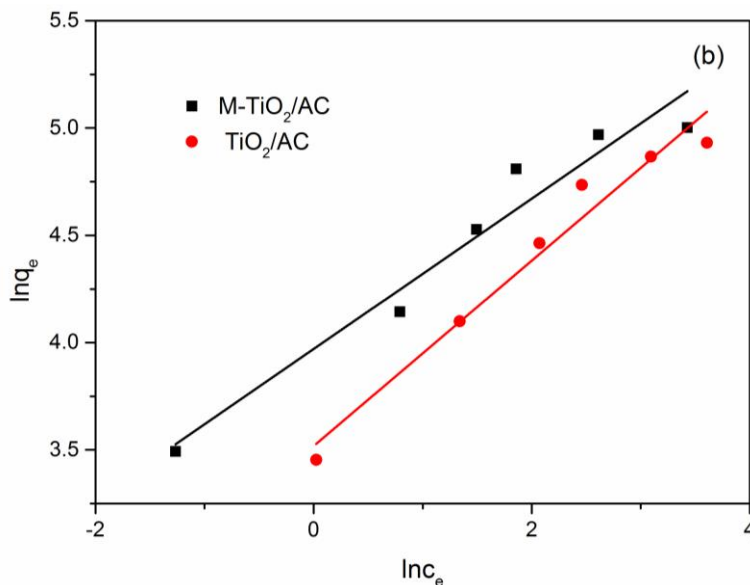


Fig. 10. Linear plots of Langmuir equation (a) and Freundlich equation (b)

Table 3. Parameters of Langmuir and Freundlich Isotherms of Samples

Samples	Langmuir			Freundlich		
	$q_m(\text{mg}\cdot\text{g}^{-1})$	$b(\text{L}\cdot\text{mg}^{-1})$	R^2	n	k_f	R^2
M-TiO ₂ /AC	161.3	0.43	0.993	2.85	52.9	0.95
TiO ₂ /AC	158.7	0.19	0.995	2.31	33.7	0.97

Note: q_m : the maximum adsorption capacity; b : the Langmuir constant related to the energy or net enthalpy of adsorption; n : the Freundlich constant represented the degree of adsorption dependence at equilibrium concentration; k_f : the Freundlich constant related to adsorption capacity and adsorption intensity; and R^2 : regression coefficient

As shown in Fig. 10 and Table 3, the adsorption isotherms of Acid Red 18 adsorption followed the isothermal adsorption equation of Langmuir Eq. 4 and Freundlich Eq. 5. Two isothermal adsorption equations were written as follows,

$$c_e / q_e = 1 / (q_m \times b) + c_e / q_m \quad (4)$$

$$q_e = K_f \times C_e^{1/n} \quad (5)$$

where c_e is the equilibrium concentration ($\text{mg}\cdot\text{L}^{-1}$), q_e is the equilibrium amount of Acid Red 18 ($\text{mg}\cdot\text{g}^{-1}$) adsorbed, and q_m is the maximum adsorption capacity ($\text{mg}\cdot\text{g}^{-1}$).

These results revealed that the present data could be a good fit in both the Langmuir and Freundlich models for Acid Red 18 adsorption. Typically when both models fit the data well, it means that too narrow a range of concentrations was considered. Therefore, the authors will study this issue in further studies. (Zhou *et al.* 2011).

Effect of Dosage of Samples

As shown in Fig. 11, the removal rate of Acid Red 18 first increased and then tended to gradually stabilize with an increased dosage of samples. This result suggested that higher dosages of samples supplied more surface adsorption points of AC and catalytic activity points of M-TiO₂/TiO₂. However, when the dosage of samples reached the saturation point in photocatalytic degradation and active carbon adsorption, the collisional frequency increased with the increase of sample particle concentration that could interfere with the absorption effect of the degradation substances. Therefore, an M-TiO₂/AC dosage of 0.15 g was appropriate for considerations of removal efficiency and economic factor.

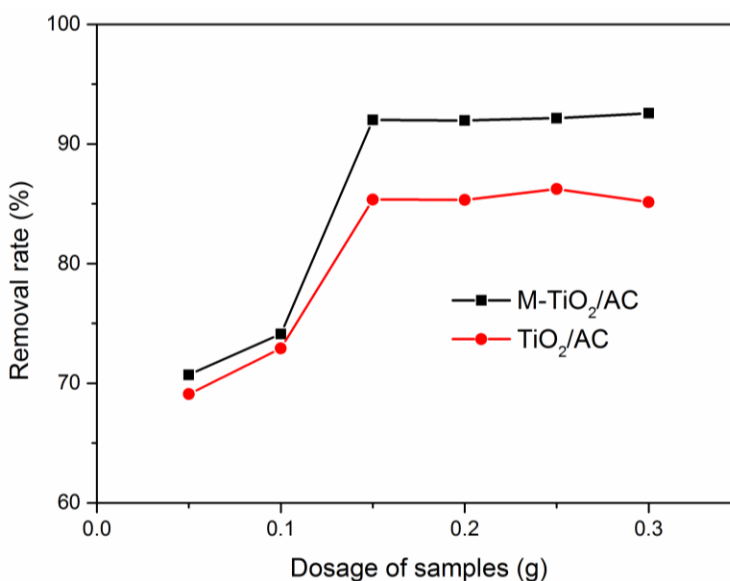


Fig. 11. Effect of dosage of samples on adsorption of Acid Red 18 solution (Acid Red 18 concentration = 80 mg·L⁻¹)

UV-vis Spectra of Acid Red 18 Solution

Figure 12 clearly shows the UV-vis spectra of the degradation process in Acid Red 18 solution with M-TiO₂/AC. There were absorption peaks at 503 nm, which represented -N=N- bonds of azo-conjugated systems and chromophore groups of the Acid Red 18 solution (Parsa *et al.* 2014). Furthermore, these absorption peaks dramatically decreased with increased contact time, which revealed that these chromophore groups were gradually damaged. Then, no new absorption peaks appeared, indicating that no new organic function regiment was generated during the degradation process. This result can be attributed to the oxidation of Acid Red 18 and decomposition into small molecular substances, such as CO₂ and H₂O, *via* strong oxidizing free hydroxyl radicals that came from M-TiO₂.

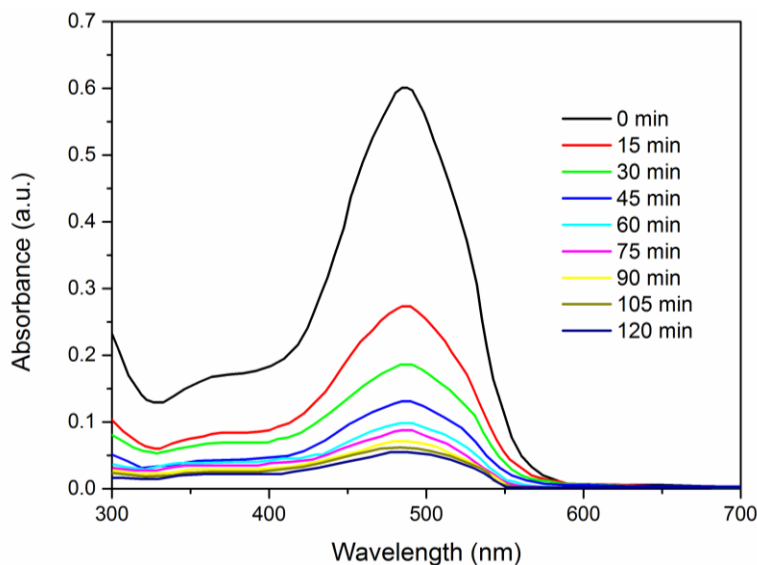


Fig. 12. UV–vis spectra of degradation process in Acid Red 18 solution with M-TiO₂/AC (Acid Red 18 concentration = 80 mg·L⁻¹; sample dosage = 0.15 g)

CONCLUSIONS

1. In this study, ordered mesoporous TiO₂ loaded onto walnut shell-based activated carbon was synthesized *via* sol-gel and ultrasonic-assisted technology. The addition of CTAB surfactant promoted the conversion of TiO₂ nanoparticles from anatase to rutile. Furthermore, the specific area of M-TiO₂/AC increased from 563 m²·g⁻¹ to 881 m²·g⁻¹, compared to TiO₂/AC, which was mainly due to the ordered mesoporous structure and large specific area (112 m²·g⁻¹) of M-TiO₂ in the pore-pore load.
2. The results revealed that the optimal adsorption and photocatalysis condition was the Acid Red 18 with a concentration of 80 mg·L⁻¹ subjected to illumination for 2 h in the presence of 0.15 g of M-TiO₂/AC. The removal rate of Acid Red 18 solution by M-TiO₂/AC reached 92.3% under this condition, which was higher than that of TiO₂/AC (83.7%), or AC (73.1%).
3. This adsorption and photocatalytic process followed the pseudo-second-order kinetic model. It involved internal diffusion and external diffusion. Acid Red 18 might be oxidized and decomposed into small molecular substances, such as CO₂ and H₂O, by strong oxidizing free hydroxyl radicals provided during the photocatalytic process by M-TiO₂.

ACKNOWLEDGMENTS

This study was supported by the National Natural Science Foundation of China (No. 51572028), the National High Technology Research and Development Program of China (863 Program, No. 2015AA033905), and the Beijing Training Project for the Leading Talents in S & T (No. 201424).

REFERENCES CITED

- Ahmaruzzaman, M., and Gupta V. K. (2011). "Rice husk and its ash as low-cost adsorbents in water and wastewater treatment," *Industrial & Engineering Chemistry Research* 50(24), 13589-13613. DOI: 10.1021/ie201477c
- Ambrus, Z., Mogyorósi, K., Szalai, Á., Alapi, T., Demeter, K., Dombi, A., and Sipos, P. (2008). "Low temperature synthesis, characterization and substrate-dependent photocatalytic activity of nanocrystalline TiO₂ with tailor-made rutile to anatase ratio," *Applied Catalysis A: General* 340(2), 153-161. DOI: 10.1016/j.apcata.2008.02.010
- Chandraboss, V. L., Kamalakkannan, J., and Senthilvelan, S. (2016). "Synthesis of activated charcoal supported Bi-doped TiO₂ nanocomposite under solar light irradiation for enhanced photocatalytic activity," *Applied Surface Science* 387, 944-956. DOI: 10.1016/j.apsusc.2016.06.110
- Fu, X., Yang, H., Lu, G., Tu, Y., and Wu, J. (2015). "Improved performance of surface functionalized TiO₂/activated carbon for adsorption-photocatalytic reduction of Cr(VI) in aqueous solution," *Materials Science in Semiconductor Processing* 39, 362-370. DOI: 10.1016/j.mssp.2015.05.034
- Fu, X., Yang, H., Sun, H., Lu, G., and Wu, J. (2016). "The multiple roles of ethylenediamine modification at TiO₂/activated carbon in determining adsorption and visible-light-driven photoreduction of aqueous Cr(VI)," *Journal of Alloys and Compounds* 662, 165-172. DOI: 10.1016/j.jallcom.2015.12.019
- Gupta, V. K., Jain R., Mittal A., Saleh T. A., and Nayak, A. (2012). "Photocatalytic degradation of toxic dye amaranth on TiO₂/UV in aqueous suspensions," *Materials Science and Engineering C* 32(1), 12-17. DOI: 10.1016/j.msec.2011.08.018
- Hubbe, M. A., Beck, K. R., O'Neal, W. G., and Sharma, Y. C. (2012). "Cellulosic substrates for removal of pollutants from aqueous systems: A review. 2. Dyes," *BioResources* 7(2), 2592-2687. DOI: 10.15376/biores.7.2.2592-2687
- Kuo, Y. L., Su, T. L., Kung, F. C., and Wu, T. J. (2011). "A study of parameter setting and characterization of visible-light driven nitrogen-modified commercial TiO₂ photocatalysts," *Journal of Hazardous Materials* 190(1-3), 938-944. DOI: 10.1016/j.jhazmat.2011.04.031
- Li, D., Ma, X., Liu, X., and Yu, L. (2013). "Preparation and characterization of nano-TiO₂ loaded bamboo-based activated carbon fibers by H₂O activation," *BioResources* 9(1), 602-612. DOI: 10.15376/biores.9.1.602-612
- Li, K., Dong, C., Zhang, Y., Wei, H., Zhao, F., and Wang, Q. (2014). "Ag-AgBr/CaWO₄ composite microsphere as an efficient photocatalyst for degradation of Acid Red 18 under visible light irradiation: Affecting factors, kinetics and mechanism," *Journal of Molecular Catalysis A: Chemical* 394, 105-113. DOI: 10.1016/j.molcata.2014.03.014
- Liu, C., Li, Y., Xu, P., Li, M., and Zeng, M. (2015). "Controlled synthesis of ordered mesoporous TiO₂-supported on activated carbon and pore-pore synergistic photocatalytic performance," *Materials Chemistry and Physics* 149-150, 69-76. DOI: 10.1016/j.matchemphys.2014.09.034
- Liu, S. X., Chen, X. Y., and Chen, X. (2007). "A TiO₂/AC composite photocatalyst with high activity and easy separation prepared by a hydrothermal method," *Journal of Hazardous Materials* 143(1-2), 257-263. DOI: 10.1016/j.jhazmat.2006.09.026
- Matos, J., Laine, J., and Herrmann, J. M. (1998). "Synergy effect in the photocatalytic degradation of phenol on a suspended mixture of titania and activated carbon,"

- Applied Catalysis B Environmental* 18(3–4), 281-291. DOI: 10.1016/S0926-3373(98)00051-4
- Mittal, A., Jhare, D., Mittal J., and Gupta, V. K. (2012). “Batch and bulk removal of hazardous colouring agent rose bengal by adsorption over bottom ash,” *RSC Advances* 2(22), 8381-8389. DOI: 10.1039/C2RA21351F
- Mittal, A., Mittal, J., Malviya, A., and Gupta V. K. (2009). “Adsorptive removal of hazardous anionic dye Congo red from wastewater using waste materials and recovery by desorption,” *Journal of Colloid and Interface Science* 340(1), 16-26. DOI: <https://doi.org/10.1016/j.jcis.2009.08.019>
- Omri, A., Lambert, S. D., Geens, J., Bennour, F., and Benzina, M. (2014). “Synthesis, surface characterization and photocatalytic activity of TiO₂ supported on almond shell activated carbon,” *Journal of Materials Science & Technology* 30(9), 894-902. DOI: 10.1016/j.jmst.2014.04.007
- Parsa, J. B., Golmirzaei, M., and Abbasi, M. (2014). “Degradation of azo dye C.I. Acid Red 18 in aqueous solution by ozone-electrolysis process,” *Journal of Industrial and Engineering Chemistry* 20(2), 689-694. DOI: 10.1016/j.jiec.2013.05.034
- Qian, L., Yang, S., Hong, W., Chen, P., and Yao, X. (2016). “Synthesis of biomorphic charcoal/TiO₂ composites from moso bamboo templates for absorbing microwave,” *BioResources* 11(3), 7078-7090. DOI: 10.15376/biores.11.3.7078-7090
- Saleh, T. A., and Gupta, V. K. (2012). “Column with CNT/magnesium oxide composite for lead(II) removal from water,” *Environmental Science and Pollution Research* 19(4), 1224-1228. DOI: 10.1007/s11356-011-0670-6
- Saravanan, R., Gupta, V. K., Mosquera, E., and Gracia, F. (2014). “Preparation and characterization of V₂O₅/ZnO nanocomposite system for photocatalytic application,” *Journal of Molecular Liquids* 198, 409-412. DOI: <https://doi.org/10.1016/j.molliq.2014.07.030>
- Senthilraja, A., Subash, B., Dhatshanamurthi, P., Swaminathan, M., and Shanthi, M. (2015). “Photocatalytic detoxification of Acid Red 18 by modified ZnO catalyst under sunlight irradiation,” *Spectrochim Acta Part A: Molecular and Biomolecular Spectroscopy* 138, 31-37. DOI: 10.1016/j.saa.2014.11.006
- Singh, P., Vishnu, M. C., Sharma, K. K., Borthakur, A., Srivastava, P., Pal, D. B., Tiwary, D., and Mishra, P. K. (2016). “Photocatalytic degradation of Acid Red dye stuff in the presence of activated carbon-TiO₂ composite and its kinetic enumeration,” *Journal of Water Process Engineering* 12, 20-31. DOI: 10.1016/j.jwpe.2016.04.007
- Wu, P., Xia, L., Dai, M., Lin, L., and Song, S. (2016). “Electrosorption of fluoride on TiO₂-loaded activated carbon in water,” *Colloids and Surfaces A: Physicochemical and Engineering Aspects* 502, 66-73. DOI: 10.1016/j.colsurfa.2016.05.020
- Xu, D., Gu, C., and Chen, X. (2013). “Adsorption and removal of Acid Red 3R from aqueous solution using flocculent humic acid isolated from lignite,” *Procedia Environmental Sciences* 18, 127-134. DOI: 10.1016/j.proenv.2013.04.017
- Xue, G., Liu, H., Chen, Q., Hills, C., Tyrer, M., and Innocent, F. (2011). “Synergy between surface adsorption and photocatalysis during degradation of humic acid on TiO₂/activated carbon composites,” *Journal of Hazardous Materials* 186(1), 765-772. DOI: 10.1016/j.jhazmat.2010.11.063
- Yu, J. G., Su, Y. R., and Cheng, B. (2007). “Template-free fabrication and enhanced photocatalytic activity of hierarchical macro-/mesoporous titania,” *Advanced Functional Materials* 17(12), 1984-1990. DOI: 10.1002/adfm.200600933

- Zhang, J., Jin, X. J., Gao, J. M., and Zhang, X. D. (2013). "Phenol adsorption on nitrogen-enriched activated carbon prepared from bamboo residues," *BioResources* 9(1), 969-983. DOI: 10.15376/biores.9.1.969-983
- Zhang, J., Shang, T., Jin, X., Gao, J., and Zhao, Q. (2015). "Study of chromium(VI) removal from aqueous solution using nitrogen-enriched activated carbon based bamboo processing residues," *RSC Advances* 5(1), 784-790. DOI: 10.1039/c4ra11016a
- Zhang, W., Zou, L., and Wang, L. (2011). "A novel charge-driven self-assembly method to prepare visible-light sensitive TiO₂/activated carbon composites for dissolved organic compound removal," *Chemical Engineering Journal* 168(1), 485-492. DOI: 10.1016/j.cej.2011.01.061
- Zhou, W., Sun, F., Pan, K., Tian, G., Jiang, B., Ren, Z., Tian, C., and Fu, H. (2011). "Well-ordered large-pore mesoporous anatase TiO₂ with remarkably high thermal stability and improved crystallinity: Preparation, characterization, and photocatalytic performance," *Advanced Functional Materials* 21(10), 1922-1930. DOI: 10.1002/adfm.201002535

Article submitted: July 21, 2017; Peer review completed: October 1, 2017; Revisions accepted: October 7, 2017; Published: October 13, 2017.
DOI: 10.15376/biores.12.4.9086-9102